# An efficient CAD projector for X-ray projection based 3D inspection with the ASTRA Toolbox

Árpád Marinovszki<sup>1</sup>, Jan De Beenhouwer<sup>1</sup>, Jan Sijbers<sup>1</sup>

<sup>1</sup>imec-Vision Lab, Department of Physics, University of Antwerp, Universiteitsplein 1, Antwerp 2610, Belgium e-mail: {arpad.marinovszki, jan.debeenhouwer, jan.sijbers}@uantwerpen.be

#### **Abstract**

An efficient X-ray projector for the ASTRA Toolbox is presented that is capable of simulating X-ray radiographs directly from CAD data in STL format. The projector is implemented on the GPU using the Nvidia OptiX framework. It can be used in 3D X-ray inspection tasks or projection-based metrology. To that end, we developed a framework for the 3D registration of CAD models to few-view projection data. The efficiency of the projector is quantified and the registration framework is evaluated on simulated and measured projection data. Finally, an example of 3D CAD based X-ray inspection is shown.

Keywords: CAD, metrology, X-ray, 3D inspection

#### 1 Introduction

3D Computed Tomography (CT) is a powerful, non-destructive technique that allows computing cross-sectional images of an object from a large set of acquired X-ray projection images using a reconstruction algorithm. It is increasingly used in dimensional metrology to inspect the deviation of the measured geometry from the nominal geometry. The latter is usually defined in Computer Aided Design (CAD) models. Conventional X-ray based inspection methods first generate a 3D image of the object to be inspected. Subsequently, the reconstructed volume is segmented, after which the surface of the object is extracted through edge detection of the binary volume. Finally, a CAD model of the object is registered to the 3D (voxelbased) reconstructed image in order to perform the analysis. The accuracy of the final analysis directly depends on the reconstructed image quality, which is influenced by object parameters (material, size, shape), measurement setup (orientation, magnification, machine settings, temperature) and data processing (reconstruction, edge detection, calibration, alignment with CAD models) [1]. That is, the conventional CAD based X-ray inspection processing pipeline is a multistep procedure that can suffer from substantial error propagation.

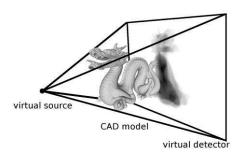


Figure 1: A simulation setup with a virtual source, a triangle mesh of a CAD model and a virtual detector.

An alternative to the conventional inspection approach is to perform (part of) the 3D inspection in projection space [2], by creating realistic radiographs of a CAD model, which are then directly compared to measured X-ray images. The procedure requires a reliable method to generate projections of 3D CAD models and to register the 3D objects to the acquired 2D projections [3]. As a first step towards projection-based inspection, we developed a CAD projector, capable of simulating X-ray radiographs directly from CAD data. The projector was accelerated with a GPU implementation using the Nvidia OptiX ray tracing engine [8,9] and is integrated in our X-ray reconstruction framework, the ASTRA Toolbox [5-7]. We propose to use the CAD projector for 3D projection-based inspection, by combining it with a 3D registration framework that estimates the 3D position and orientation of the CAD model from few-view projection data.

#### 2 Methods

We propose a workflow for fast X-ray projection-based inspection. In section 2.1, we introduce the reader to the algorithms we use to create realistic projections of the CAD models. First, we describe how the acquisition geometry is set up and used to calculate line lengths a ray travels inside the CAD object between the source and the detector pixels. Next, in section 2.2, we show methods to convert the calculated line lengths to realistically looking projection images. In section 2.3, we show how the X-ray spectrum of the imaging system is estimated during 3D registration to projection data for both simulated and measured data. In section 2.4, an example of 3D X-ray inspection is shown to illustrate the potential of the method.

### 2.1 Calculating line lengths

The CAD projector is an extension to the ASTRA Toolbox, an open source tomographic framework [5-7]. With the current improvements, the toolbox is now able to create simulated X-ray images, based on CAD files in STL (STereoLithography) file format. Such files describe the surface of an object by dividing it into triangles. First, this triangle mesh is loaded into the Nvidia Optix engine, which is a general purpose, GPU accelerated raytracing library. We use this framework due to its capabilities of

executing raytracing tasks parallelized on the GPU, while it has a high level programming interface. The loaded triangle mesh is stored in the memory of the graphics card encapsulated in abstract accelerated structures. Next, the projection geometry is defined by specifying the trajectory of the virtual source and the virtual flat panel detector in the coordinate system of the CAD model. The size and the number of detector pixels also have to be set. The defined geometry therefore describes a cone beam setup, as depicted in Figure 1. The projection geometry is defined using the flexible tool sets that are already built in the ASTRA Toolbox. Therefore it is easy to define conventional circular source and detector trajectories, as well as specifying unique geometries, such as tomosynthesis, laminography, or a conveyor belt setup.

Once the triangle mesh and the acquisition geometry are defined, the Optix library is used to cast rays from the X-ray source to the middle of each detector pixel. It detects collisions between the rays and the triangle mesh, and calculates the distance a ray travels within the CAD model. First intersection points between the ray and the bounding box of the triangles are calculated using the built-in functionalities of the Optix library. The exact location of the intersection is determined using our implementation of a watertight ray-triangle intersection algorithm described in [4]. The cited method determines whether the ray actually has an intersection with a given triangle, and also calculates the distance between the point of intersection and the source of the ray. We use these distances to calculate the distance the ray travels within the volume. Assuming that the triangle mesh represents a closed object, it is determined as the difference of the distances between the source and every second point of intersection.

The usage of the line length calculation algorithm is similar to the rest of the various reconstruction and forward- and backprojection methods in the ASTRA Toolbox. The user can interact with the high level Matlab interface, whereas the calculations are executed on the GPU.

# 2.2 Creating polychromatic projections

From the calculated line lengths, realistically looking projections of the CAD model are synthesized. We formulate the problem using a polychromatic adaptation of the Lambert-Beer law, using the notations of [8]:

$$I = I_0 \int_{E_{\min}}^{E_{\max}} D(E) \ s(E) \ e^{-\int_L \mu(E,r) dl} dE , \qquad (1)$$

where **E** is the photon energy and  $\mathbf{E}_{min}$  and  $\mathbf{E}_{max}$  are the minimum and maximum photon energies,  $\mathbf{s}(\mathbf{E})$  is the normalized spectrum of the source,  $\mathbf{D}(\mathbf{E})$  is the product of the detector response function, and any filter that may be present in the imaging setup, **L** is the path from the source to a given detector pixel, and **I** is the measured intensity value. After discretization and introducing two new variables,  $\mathbf{W}(\mathbf{E}) = \mathbf{I}_0 \mathbf{D}(\mathbf{E}) \mathbf{s}(\mathbf{E})$  and  $\mathbf{A}_i = \mathbf{e}^{-\sum_j \int_L \mu_j(\mathbf{E}_i, \mathbf{r}) dl}$ , Equation (1) becomes

$$I = \sum_{i} W(E_i) A_i \Delta E_i , \qquad (2)$$

where  $W(E_i)$  is the effective spectrum, i.e. a weight of the i-th energy bin, which is evaluated at energy  $\Delta E_i$ . It also incorporates the effect of all energy dependent processes in the imaging system.  $A_i$  is a monochromatic projection image, evaluated at energy  $E_i$ .  $\Delta E_i$  is the width of the i-th energy bin. The effective spectrum  $W(E_i)$  and  $\Delta E_i$  are therefore independent of the phantom being imaged and they are strictly dependent on the imaging setup and the resolution of the discretized spectrum. The estimation of these parameters is discussed in section 2.3.

The factor in Equation (2) that is related to the CAD model being imaged is  $A_i$ . It can be computed as

$$A_i = e^{-\sum_j \mu_j(E_i)L_j},\tag{3}$$

where  $L_j$  is the line length of the ray within material j. In conclusion, we propose to synthesize realistic images using the following scheme:

- 1. Calculate the line lengths of each single-material CAD model  $(L_i)$  using the ASTRA Toolbox.
- 2. Create the mono-energetic images  $(A_i)$  according to Equation (3).
- 3. Calculate the final intensity values using Equation (2).

## 2.3 Estimating the spectrum

In order to efficiently compare the CAD projections with real radiographs, the energy spectrum and the detector response of the imaging system, i.e. term  $W(E_i)$  in Equation (2), must be known. This quantity, however, depends on many factors, such as the materials and the geometry of the X-ray source and the detector, the applied source filter, etc. The precise measurement of this term can be a complex process, requiring specialized measuring equipment. However, the spectrum can also be approximately estimated by measuring the intensity values on the projections of a phantom with a known material and thickness. The method described in [10] uses the projections of a polycarbonate and an aluminium step-wedge phantom for this purpose. Based on the attenuation values and the thickness of the different parts of the phantom, Duan et al. calculate the term  $A_i$ , introduced in Equation

(2). Then, an Expectation Maximization algorithm is used to solve the linear equation system (2) for the effective spectrum  $W(E_i)$ .

The spectrum estimation method we propose is similar to the one of Duan et al [10], with the difference of using a man-made product, of which we have a CAD model and its material specification, as a phantom. In this process, the term  $A_i$  is calculated using the CAD model, according to Equation (3). Then, similar to the above mentioned approach, X-ray images are taken of the product and the effective spectrum  $W(E_i)$  is calculated by solving the equation system (2). For this step, instead of using the proposed Expectation Maximization algorithm, we used a convex optimization toolbox [11], to solve the problem defined in Equation (4). In contrast to the EM method, which needs a close initial guess to converge to the optimal solution, the optimization based approach does not require initialization.

$$W(E_i) = \underset{W(E_i)}{\operatorname{argmin}} \|I - \sum_i W(E_i) A_i \Delta E_i\|_2. \tag{4}$$

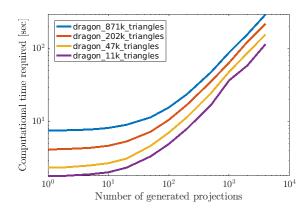
The method relies on the knowledge of the thickness of different materials in the product, along each line between the source and the different pixels of the detector. To use these line lengths according to Equation (2) and (4), it is required to measure the line lengths using the same acquisition geometry, as the reference projections I are measured.

Even if the acquisition geometry is known, misalignments of the product, such as tilt, rotation, translation, may result in poor spectrum estimation. In these cases, the trajectories of the rays that the CAD model projector uses to calculate the line lengths may differ from the trajectory of the X-ray beam in the actual acquisition process. Therefore, a method is needed to register the posture of the physical object to the CAD model in the simulation environment. For this purpose, a projection based 2D-3D registration approach similar to [3] was developed to correct for misalignments. After registration, the quality of the inspected object can be evaluated by comparing its simulated projection data to the simulated or measured sample data.

# 3 Experiments and results

# 3.1 Computational speed of the CAD projector

We evaluated the speed of the CAD projector process, that was described in section 2.1, in function of the number of detector pixels as well as the number of triangles in the CAD model and the number of projections. For these studies, we used the 'dragon' CAD model from the library of the Stanford University Computer Graphics Laboratory. The model is available in 4 different resolutions. They contain around 871k, 202k, 48k and 11k triangles, respectively. The most detailed 3D dragon model and its simulated projection is illustrated in Figure 1.



political particular dragon\_871k\_triangles dragon\_202k\_triangles dragon\_47k\_triangles dragon\_11k\_triangles dragon\_11k\_triangles dragon\_11k\_triangles dragon\_11k\_triangles

Figure 2: Computation time as function of the number of projections.

Figure 3: Computation time as function of the number of detector pixels.

The computation time as function of the number of projections for the different models with a fixed (1000x1000 pixels) detector size was measured on an NVidia Tesla K80 graphical processing unit and an Intel Xenon E5-2620 v4 central processing unit. The results are shown in Figure 2. Similarly, the computation time for projecting a batch of 1000 projections in function of the number of detector pixels is shown in Figure 3. These results illustrate the overhead of the Optix library to create accelerated data structures while the triangle mesh is loaded. The computation time is proportional to the size of the mesh and it causes a small amount of projections to be generated relatively slowly. However, once the mesh is loaded, the computation time is almost independent of the size of the mesh and if enough projections are generated to make use of the parallel architecture, it is nearly proportional to the number of generated pixels.

# 3.2 Estimation of the effective source spectrum of an imaging system using CAD models

The spectrum estimation method described in section 2.3 was first evaluated on simulated data with known circular cone beam acquisition geometry (i.e. without introducing misalignment). Polychromatic projections of a CAD model were generated, using the scheme described in section 2.2. For this study, a generic ground truth spectrum was used with 180kV peak voltage. The spectrum, shown in Figure 4 was binned to 180 bins of 1keV. As a phantom, the CAD model of a medical device, the K-pack Surshield needle, produced by Terumo Europe NV was used. It consists of 10 different parts, which are made of various types of polymers and steel. The CAD model and one of the simulated ground truth projections are shown in Figure 4.

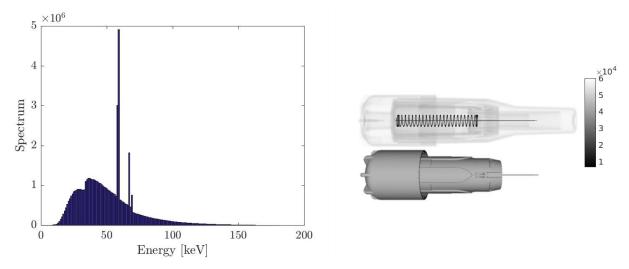


Figure 4: Ground truth spectrum (left) and the 3D CAD model along with an example polychromatic projection (right).

Next, the spectrum was estimated using a different number of projections and energy bins in the recovered spectrum. In each case, the projection angles were evenly distributed on the interval  $[0^{\circ}, 360^{\circ})$ . The width of the energy bins was adjusted to the number of energy bins, such that each bin within the energy range [0,180keV] had the same width. To test the accuracy of spectrum estimation, we simulated projections using the estimated spectrum and measured their mean square error (MSE) to the ground truth projections. The results are shown in Table 1. It is clear that a very low MSE can be achieved, which indicates that the unknown spectrum is estimated well with respect to the energy bins that are required to approximate the projection data intensity values of this specific sample.

MSE			Number of energy bins					
	of		2	36	72	108	144	180
projections		1	4.35E+5	5.36E-3	3.88E-6	7.39E-7	7.95E-7	2.30E-7
		2	4.39E+5	5.48E-3	4.83E-6	6.03E-7	1.27E-6	6.96E-7
		4	4.40E+5	5.15E-3	3.60E-6	5.10E-7	1.83E-6	2.16E-6
		6	4.39E+5	5.19E-3	1.23E-5	4.53E-7	1.83E-6	1.98E-6
		10	4.40E+5	5.21E-3	3.96E-6	6.51E-7	1.05E-5	3.04E-6
		14	4.40E+5	5.18E-3	3.33E-6	7.75E-7	1.92E-6	3.75E-6
		18	4.40E+5	5.21E-3	3.62E-6	8.40E-6	1.85E-6	1.18E-5

Table 1: Spectrum estimation accuracy expressed as the projection distance (MSE) between the simulated polychromatic forward projection and the ground truth projection data.

Due to the fact that the sample itself is rotationally symmetric (constraining the variety of line lengths) and contains only a limited amount of materials, it is obvious that the spectrum estimation method cannot recover the full spectrum. However, as

Figures 5 and 6 clearly show, this is not required in order to match the projection data of a specific sample and an excellent agreement can already be found with less than 18 projections and as few as 36 energy bins. The specific amount of data required to approximate the spectrum will however be sample dependant. It is therefore expected that it is beneficial to estimate the spectrum from a variety of different samples with 108 or more energy bins to obtain a closer agreement to the true spectrum if a large variety or different samples are to be inspected.

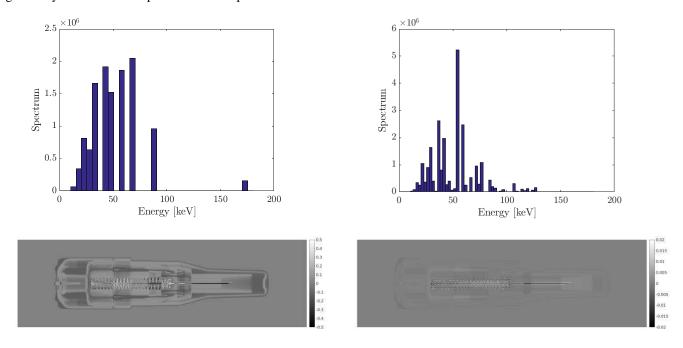


Figure 5: Spectrum estimation and difference image of a single CAD projection with the ground truth for 32 energy bins (left) and 72 energy bins (right).

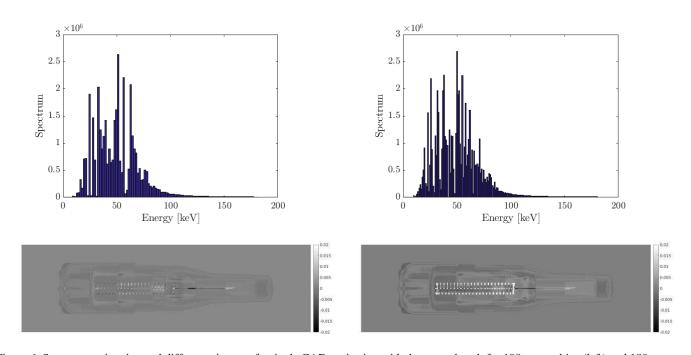


Figure 6: Spectrum estimation and difference image of a single CAD projection with the ground truth for 108 energy bins (left) and 180 energy bins (right).

Finally, the CAD model based spectrum estimation and the 2D-3D registration of CAD data to projections are combined to approximate the intensity values of experimentally measured projection data. For this experiment, a real K-pack Surshield needle was used of which 35 projections of 966 by 752 pixels were acquired over 360° with a pixel size of 74.8 micron. The source to detector distance was 765mm and the source to object distance was 489.4mm. A CAD model of the spring and needle was not taken into account for the registration and spectrum estimation. The spectrum estimation and registration was performed with a subset of 18 projections and for 108 energy bins. The results in Figure 7 clearly show an excellent agreement for both the registration and the intensity values of the projection data. This result clearly indicates the potential of our method for non-destructive testing and quality control using 3D registered projection data.

#### 4 Conclusions

We demonstrated a GPU-based CAD projector along with an automated procedure to approximate the intensity values of few-view measured projection data by estimating the spectrum of a polychromatic X-ray source using 3D registered CAD data and material specifications as prior knowledge. We also described how our method can be used in the field of non-destructive testing.

Figure 7: Simultaneous spectrum and 3D registration estimation with 108 energy bins of experimentally measured projection data. A single measured projection is shown (top) along with its corresponding 3D registered CAD projection (middle) and a difference image (bottom).

# 5 Acknowledgements

This research is funded by the imec ICON project iXCon (Agentschap Innoveren en Ondernemen project nr. HBC.2016.0164) and the FWO SBO project MetroFlex (S004217N). The authors would like to thank Terumo Europe for providing the CAD models and the K-pack sample and also XRE NV for acquiring the projection data.

#### References

- [1] Welkenhuyzen F., Kiekens K, Pierlet M., Dewulf W., Bleys P., Kruth, J-P. Voet A, "Industrial computed tomography for dimensional metrology: overview of influence factors and improvement strategies", 4th Int. Conf. on Optical Measurement Techniques, 401–10, (2009)
- [2] J. A. Noble, R. Gupta, J. Mundy, A. Schmitz and R. I. Hartley, High precision X-ray stereo for automated 3D CAD-based inspection, IEEE Transactions on Robotics and Automation, vol. 14, no. 2, pp. 292-302, Apr 1998.
- [3] S. Miao, A. Tuysuzoglu, Z.J. Wang, R. Liao, Real-time 6DoF pose recovery from X-ray images using library-based DRR and hybrid optimization, International Journal of Computer Assisted Radiology and Surgery, vol. 11, pp. 1211—1220, 2016.
- [4] S. Woop, C. Benthin, and I. Wald, Watertight ray/triangle intersection., Journal of Computer Graphics Techniques (JCGT) 2.1 (2013): 65-82.
- [5] W. van Aarle, Palenstijn WJ, Cant J, Janssens E, Bleichrodt F, Dabravolski A, De Beenhouwer J, Batenburg J, Sijbers J, Fast and Flexible X-ray Tomography Using the ASTRA Toolbox, Optics Express, 24(22), pp. 25129-25147, 2016.
- [6] W. van Aarle, W. J. Palenstijn, J. De Beenhouwer, T. Altantzis, S. Bals, K. J. Batenburg, and J. Sijbers, "The ASTRA Toolbox: a platform for advanced algorithm development in electron tomography", Ultramicroscopy, Vol. 147, p. 35–47, (2015)
- [7] W J. Palenstijn, K J. Batenburg, and J. Sijbers, "Performance improvements for iterative electron tomography reconstruction using graphics processing units (GPUs)", Journal of structural biology, vol. 176, nr 2, pp. 250-253, 2011
- [8] N. Freud, P. Duvauchelle, J.M. Létang and D. Babot, Fast and robust ray casting algorithms for virtual X-ray imaging, Nuclear Instruments and Methods in Physics Research Section B, Vol. 248, pp. 175-180, 2006.
- [9] S.G. Parker, et al., Optix: a general purpose ray tracing engine., ACM Transactions on Graphics (TOG), Vol. 29. No. 4. ACM, 2010.
- [10] X. Duan, J. Wang, L.Yu, S. Leng and C.H. McCollough, CT scanner x-ray spectrum estimation from transmission measurements. Medical Physics, Vol. 38 No. 2, 2011.
- [11] Michael Grant and Stephen Boyd. CVX: Matlab software for disciplined convex programming, version 2.1 http://cvxr.com/cvx, March 2017.